

Alexandria Journal of Science and Technology



Article

An Efficient Novel Linker for Cu-MOF Design: Remediation of Congo Red (CR) and Tropaeolin OO (TOO) as Organic Pollutants

Marawan M. Ramadan, Azza M. Shaker, Mohamed Hagar, Ahmed R. Rabee, Hanaa Rasheed, Amira H. E. Moustafa³

Department of Chemistry, Faculty of Science, Alexandria University, P.O. Box 426, Alexandria, 21321, Egypt.

* Correspondence Address:

Amira H. E. Moustafa: Department of Chemistry, Faculty of Science, Alexandria University, P.O. Box 426, Alexandria, 21321, Egypt. Email: amira.mostafa@alexu.edu.eg.

KEYWORDS: Cu-MOF; Organic linkers; azo dyes; isotherms; Reusability.

Received:

June 30, 2025

Accepted:

September 23, 2025

Published:

November 17, 2025

ABSTRACT: The widespread discharge of synthetic dyes into aquatic environments poses a serious threat to ecosystems, water quality, and public health. In this study, a copper-based metal-organic framework (Cu-MOF) was synthesized via a solvothermal method using an unconventional organic linker, 1,2,4-benzene-tricarboxylic anhydride (BTC). An unconventional 1,2,4-BTC linker was chosen for its adjacent carboxyl groups. This configuration enables intramolecular hydrogen bonding, which stabilizes the framework and provides additional sites for pollutant capture. The linker's identity was first confirmed by NMR. The resulting Cu-MOF was systematically characterized using Fourier Transform Infrared Spectroscopy (FTIR), X-ray Diffraction (XRD), Scanning Electron Microscopy (SEM), Transmission Electron Microscopy (TEM), Energy-Dispersive X-ray Spectroscopy (EDX), and X-ray Photoelectron Spectroscopy (XPS). These analyses confirmed the formation of a highly crystalline and porous structure, while Brunauer-Emmett-Teller (BET) measurements indicated a low N₂accessible surface area with macropores and interparticle holes. Thermogravimetric Analysis (TGA) confirmed strong thermal stability. The Cu-MOF's negative surface charge electrostatically attracted anionic dyes, enabling high removal rates of 89% for Congo Red (CR) and 85% for Tropaeolin OO. Adsorption followed pseudosecond-order kinetics, and the Temkin isotherm model indicated binding occurred on a heterogeneous surface through indirect interactions. Thermodynamic evaluations confirmed that the adsorption process was both spontaneous and endothermic. Reusability tests demonstrated that the Cu-MOF retained over 60% of its initial efficiency after five regeneration cycles, highlighting its durability. The Cu-MOF is an effective, durable, and reusable material for sustainably removing hazardous azo dyes from wastewater.

1. INTRODCTION

Water pollution caused by the discharge of synthetic dyes has emerged as a significant global environmental issue, particularly with the growth of industries such as textiles, leather, and paper manufacturing. These industries are major contributors to the release of large volumes of colored wastewater, which often contains toxic dyes that are highly resistant to natural degradation processes and can persist in aquatic environments for long periods [1].

Azo dyes, such as Congo Red (CR) and Tropaeolin OO (TOO), are widely used but are problematic due to their chemical stability, low biodegradability, and potential to form carcinogenic byproducts [2]. The presence of such dyes in water bodies not only deteriorates the aesthetic quality of the water but also disrupts aquatic life by inhibiting photosynthesis and oxygen exchange, posing serious health risks to marine

organisms and humans [3].

The removal of toxic dyes from industrial effluents is critical to mitigating environmental damage and protecting public health. Traditional methods of dye removal, including chemical oxidation, coagulation-flocculation, and membrane filtration, often encounter challenges such as high operational costs, low efficiency at low dye concentrations, and the generation of secondary pollutants [4, 5]. In contrast, adsorption has become one of the most effective and economically viable methods for removing dyes from wastewater due to its simplicity, high efficiency, and minimal generation of secondary waste [6].

The choice of adsorbent material is crucial for optimizing adsorption performance, with metal-organic frameworks (MOFs) gaining increasing attention due to their ability to selectively adsorb pollutants, such as dyes, from water [7,8]. MOFs are crystalline hybrid materials composed of metal ions coordinated with organic ligands, forming highly porous

structures that offer a large surface area and tunable functionality [9]. Copper-based MOFs (Cu-MOFs) have been especially attractive due to their relatively low cost, high stability in aqueous solutions, and versatile surface chemistry that can be tailored for specific applications in environmental remediation [10].

The organic linkers used in the synthesis of MOFs play a significant role in determining the material's adsorption properties. By selecting appropriate organic ligands, the surface charge, pore size, and chemical functionality of the MOFs can be adjusted to enhance their ability to adsorb specific pollutants such as azodyes.

In this study, a new organic linker (1,2,4-benzene-tricarboxylic anhydride) was used to synthesize a copper-based metal-organic framework (Cu-MOF) through the solvothermal method. Its efficiency has been evaluated through the removal of two anionic azo dyes, Congo red (*CR*) and Tropaeolin OO (*TOO*), from aqueous solutions. The work focuses on modifying the surface properties, pore structure, and chemical functionality of the Cu-MOF to enhance the adsorption of dyes. Key parameters, including zeta potential, kinetics, isotherms, thermodynamics, and regeneration studies, were investigated to understand the adsorption mechanisms and evaluate the sustainability and efficiency of the Cu-MOF for wastewater treatment applications.

2. Materials and methods

2.1. Materials

All chemicals and reagents used in this study were of analytical grade and were used without further purification. Congo Red (CR) and Tropaeolin OO (TOO) dves, whose molecular structures are shown in **Figure 1**, were used as model pollutants. 1,2,4-Benzene-tricarboxylic anhydride (≥ 97%) was obtained from Sigma-Aldrich and used in the synthesis of copper-based metal-organic frameworks (Cu-MOFs). Copper(II) nitrate trihydrate (Cu(NO₃)₂·3H₂O, 98%) was used as the copper source and procured from SRL India. N, N-Dimethylformamide (DMF, 99.8%) served as the primary solvent during synthesis. Additional chemicals, including sodium hydroxide (NaOH), hydrochloric acid (HCl), and Paraffinic oil, used during synthesis or preparation steps, were sourced from the Alexandria Mineral Oils Company (AMOC). Deionized water was used throughout all synthesis, washing, and experimental procedures.

2.2. Synthesis of 1,2,4-benzene tricarboxylic acid (BTC)

To synthesize the tetracarboxylic acid derivative, 1 mmol of 1,2,4-benzene-tricarboxylic anhydride (BTC) was subjected to alkaline hydrolysis. The anhydride was dissolved in a 6 N NaOH solution and refluxed at a controlled temperature of 60–80 °C for 6 h, allowing complete conversion of the anhydride groups into carboxylic acid functionalities. After cooling, the reaction mixture was gradually acidified with 1 N HCl until the pH reached 2–3, leading to the precipitation of a white solid. The product was collected by centrifugation and dried at room temperature for subsequent applications. The successful formation of the tetracarboxylic acid was further confirmed by ¹H NMR spectroscopy, as shown in **Figure S6**, which verified the expected chemical shifts corresponding to the introduction

of the additional carboxyl group. A schematic representation of the reaction is shown in **Scheme 1**.

Tropaeolin OO dye (
$$TOO$$
)

 $\lambda_{max} = 440 \text{ nm}$

(a)

 $\lambda_{max} = 400 \text{ mm}$
 $\lambda_{max} = 495 \text{ nm}$

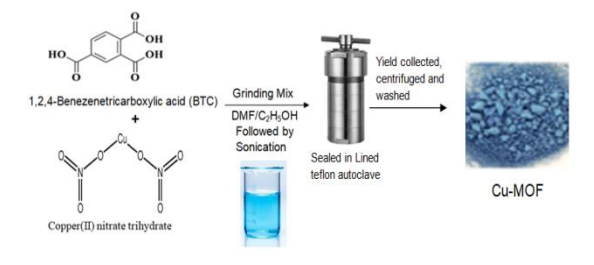
(b)

Figure 1. (a) Structure of Tropaeolin OO (*TOO*) (b) Structure of Congo Red (*CR*).

Scheme 1. Synthesis of 1,2,4-benzene tricarboxylic acid (BTC) from anhydride.

2.3. Synthesis of Cu-MOF

The Cu-MOF was synthesized using a two-step method involving mechanochemical grinding followed by solvothermal crystallization, as outlined in Scheme 2. In the initial step, copper(II) nitrate trihydrate (Cu(NO₃)₂·3H₂O, 0.496 g, 2.1 mmol) and 1,2,4-benzenetricarboxylic acid (BTC, 0.252 g, 1.05 mmol) were combined in a 2:1 molar ratio (metal to ligand) and ground manually for approximately 10 minutes to form a homogeneous mixture. The ground powder was then dispersed in a mixed solvent system consisting of N, Ndimethylformamide (DMF) and ethanol, totaling 20 mL, and stirred continuously at ambient temperature to ensure the proper dissolution and dispersion of the components. Subsequently, the suspension underwent ultrasonic treatment for 30 minutes to enhance the interaction between the copper ions and organic ligands, thereby improving the uniformity of the precursor solution. The mixture was then transferred into a Teflon-lined stainless steel autoclave and heated at 120°C for 48 hours in an oil bath under static conditions. This solvothermal process facilitated the nucleation and growth of the Cu-MOF crystals. After naturally cooling to room temperature, the solid product was collected via centrifugation at 4000 rpm and washed thoroughly with DMF to remove unreacted ligands and excess solvents. Further washing with ethanol and deionized water ensured the elimination of surface impurities. The final product was dried in an oven at 100-120 °C and stored in a vacuum desiccator to maintain its structural integrity and prevent moisture uptake. The synthesis yielded approximately 0.43 g of Cu-MOF, corresponding to a yield of around 65% relative to the total initial mass of the starting materials.



Scheme 2. Synthesis of Cu-MOF from 1, 2, 4-benzene tricarboxylic acid.

2.3.1. Reaction Mechanism

Cu-based metal-organic framework (Cu-MOF) was synthesized via a hydrothermal method using copper(II) nitrate trihydrate (Cu(NO₃)₂·3H₂O) and 1,2,4-benzenetricarboxylic acid (H₃BTC) as precursors. At elevated temperatures, the carboxylic acid groups of H₃BTC undergo deprotonation, facilitating coordination with Cu2+ ions. This deprotonation is thermodynamically favored at higher temperatures, enabling the formation of Cu-carboxylate coordination bonds, which are essential for MOF assembly. In the aqueous reaction medium, Cu2+ ions undergo partial hydrolysis to form species such as [Cu(H₂O)₂(OH)]⁺, which are stabilized by surrounding water and hydroxide ions. These species foster the formation of dinuclear Cu clusters, where two Cu(II) centers are bridged by carboxylate groups derived from deprotonated BTC ligands. These binuclear Cu clusters serve as secondary building units, linking to BTC ligands to generate the extended MOF framework structure [11].

2.4. Characterization of Cu-MOFs

The synthesized Cu-MOF was comprehensively characterized using several analytical techniques. Powder X-ray diffraction (XRD) was employed to assess the crystallinity of the framework. The morphology and surface features were examined with scanning electron microscopy (SEM, JEOL JSM-6360 LA, Japan) equipped with an energy-dispersive Xray (EDX) detector. Transmission electron microscopy (TEM) images were obtained using a JEOL JEM-2100 microscope (JEOL Ltd., Tokyo, Japan) operated at 200 kV at the Central Metallurgical Research and Development Institute (CMRDI), Cairo, Egypt. Elemental composition and surface states were analyzed by X-ray photoelectron spectroscopy (XPS, Thermo Scientific ESCALAB 250Xi VG). Functional groups and bonding interactions were identified using Fourier-transform infrared spectroscopy (FTIR, Bruker Tensor 27, Bruker Optics, Ettlingen, Germany) in the range of 4000-400 cm⁻¹ at the Central Laboratory, Faculty of Science, Alexandria University. Raman spectra were collected with a confocal micro-Raman spectrometer (alpha300 RA/S, WITec GmbH, Ulm, Germany) using a 532 nm laser, a Zeiss EC Epiplan-Neofluar 100×/0.9 objective, and a 600 g/mm grating (BLZ 500 nm) at the Egyptian Petroleum Research Institute (EPRI). Zeta potential measurements were performed with a Nano Zetasizer ZS (Malvern Instruments Ltd., Worcestershire, UK) at CMRDI.

Surface area and porosity were determined by Brunauer–Emmett–Teller (BET) analysis using BELSORP max II equipment (Japan), after outgassing the samples under vacuum (10⁻⁴ Torr) at 150 °C at the Petroleum Research Institute. Nuclear Magnetic Resonance (NMR) spectroscopy (Bruker Avance III 400 MHz, Petroleum Research Institute, Egypt) was conducted to confirm the structural identity of the organic linker. Furthermore, thermogravimetric analysis (TGA) was performed at the Central Metallurgical Research and Development Institute (CMRDI), Cairo, Egypt, using a Shimadzu DTG-60H thermal analyzer to assess the thermal stability of the Cu-MOF.

2.5. Batch adsorption experiment

The adsorption efficiency of Cu-MOF was evaluated for the removal of two synthetic dyes: CR and TOO. Stock solutions of each dye at a concentration of 1000 mg/L were prepared and subsequently diluted to achieve the desired working concentrations(5:50 ppm). Batch adsorption studies were conducted in 250 mL Erlenmeyer flasks containing 50 mL of dye solution, which were agitated at 200 rpm and maintained at a constant temperature of 25 °C. The pH of the solution was adjusted prior to Cu-MOF addition using 0.1 N NaOH or H₂SO₄, as required. A fixed mass of Cu-MOF (0.2 g) was introduced into each flask, and all experiments were performed in triplicate to ensure reproducibility. For kinetic studies, the contact time between the adsorbent and dye solutions ranged from 30 to 180 minutes. To investigate the effect of adsorbent dosage, the quantities of Cu-MOF were varied from 0.05 to 0.30 In the isotherm experiments, different initial dye concentrations were used by diluting the stock solutions accordingly. The temperature-dependent adsorption behavior was examined at temperatures ranging from 25°C to 45°C for thermodynamic analysis. The residual concentrations of CR and TOO were determined using a UV-Visible spectrophotometer at wavelengths of 495 nm and 440 nm, respectively[12]. The dye removal efficiency (%Re) and the amount of adsorbed dye (q) were calculated based on the difference between initial and final concentrations using the standard removal equations described in Table S1.

2.6. Reusability of Cu-MOFs

The reusability of the synthesized MOF was evaluated through five successive adsorption-desorption cycles using CR and TOO as model anionic dyes. Following each adsorption step, the regeneration of the spent Cu-MOF was performed using a 0.1 M sodium hydroxide (NaOH) solution as the desorbing agent. The alkaline conditions promoted surface deprotonation of the MOF, thereby weakening the electrostatic interactions between the negatively charged dye molecules and the positively charged active sites on the Cu-MOF. This process facilitated the efficient release of the adsorbed dyes. After desorption, the material was thoroughly washed with deionized water to remove the residual base, followed by centrifugation to recover the solid adsorbent. The regenerated Cu-MOF was then dried at 80-100 °C for reuse. This regeneration procedure demonstrated that the Cu-MOF retained considerable adsorption capacity for both CR and TOO over five cycles, highlighting its structural stability and potential for repeated application in dye removal from aqueous solutions.

3. Results and discussion

3.1. Morphological Feature

As shown in Figure 2a, tricarboxylic acid (trimellitic acid, TMA) shows a series of sharp and intense reflections in the lowangle region ($2\theta \approx 6-20^{\circ}$) together with multiple well-defined peaks at higher angles (20–40°). The most intense reflections are observed at approximately $2\theta \approx 6.9^{\circ}$, 9.5° , 13.6° , 15.2° , 17.5°, 19.1°, and 20.3°, indicating the formation of a crystalline framework structure. When compared with the well-known HKUST-1 $(Cu_3(BTC)_2, BTC = 1,3,5$ -benzene-tricarboxylate), the diffraction features are clearly different. HKUST-1 is characterized by a strong diagnostic reflection at $2\theta \approx 6.7^{\circ}$ (assigned to the (200) plane), followed by reflections at 9.5°, 11.6°, 13.5°, and 15.1° corresponding to the cubic Fm-3m lattice. In contrast, the Cu-TMA pattern does not reproduce the full set of HKUST-1 reflections; instead, it displays additional unique peaks in the 2θ range of $16-20^{\circ}$, consistent with reports of copper-trimellitate frameworks, where the 1,2,4-substitution pattern enforces a different connectivity and pore topology compared to the 1,3,5-isomer. These structural differences between the 1,2,4-BTC and 1,3,5-BTC linkers explain the deviation in PXRD fingerprint and confirm that the product belongs to the Cu-TMA family rather HKUST-1 [13].

A detailed investigation of the SEM images (Figure 2b) of the synthesized Cu-MOF reveals a porous, aggregated surface morphology composed of irregular crystalline clusters. This texture is characteristic of Cu-MOFs formed from polycarboxylate ligands such as 1,2,4-benzenetricarboxylic acid (BTC), which support the development of open frameworks with interconnected porosity. Such morphology is beneficial for adsorption processes, as it enhances surface accessibility and provides efficient pathways for the diffusion of guest molecules. The structural features observed align with recent studies reporting similar surface characteristics in Cu-BTC frameworks synthesized under solvothermal conditions [14]. As illustrated in Figure 2c, the EDX spectrum confirms the presence of Copper (Cu), oxygen (O), and carbon (C) with relative atomic percentages of 20.87%, 40.67%, and 37.79%, respectively, validating the successful fabrication of the Cu-MOF [15].

For better elucidation of the surface micromorphology, the TEM images of the fabricated Cu-MOF were studied in detail. Figure 2(d) revealed uniformly dispersed Cu-MOF particles with a well-defined, faceted morphology typical of BTC-based frameworks. The absence of significant agglomeration suggests a stable and consistent synthesis. This structural order, characteristic of Cu-BTC MOFs, enhances surface accessibility and supports efficient diffusion, making it suitable for adsorption applications. These results align with recent reports on Cu-MOFs exhibiting a similar morphology and dispersion [16].

The FTIR spectra presented in **Figure 2e** provide clear evidence of the stepwise transformation from the acid anhydride precursor to benzene-1,2,4-tricarboxylic acid (BTC), followed by successful coordination with copper ions to form the Cu-MOF. The spectrum of the acid anhydride exhibits characteristic C=O stretching vibrations at 1840 cm⁻¹ and 1760 cm⁻¹, indicative of the symmetric and asymmetric stretching modes of

the anhydride groups. Upon hydrolysis, these peaks disappear, and the resulting BTC exhibits a broad O-H stretching band in the range of 3600-3200 cm⁻¹, along with a strong C=O stretching vibration near 1710 cm⁻¹, confirming the presence of carboxvlic acid functionalities. Following coordination with copper (II) ions, the Cu-MOF spectrum exhibits a noticeable shift and broadening of the O-H region, now centered at 3400 cm⁻¹, reflecting the presence of hydrogen bonding and structural water. The C=O stretch of the free acid at 1710 cm⁻¹ diminishes, while two new peaks appear at 1564 cm⁻¹ and 1411 cm⁻¹, corresponding to the asymmetric and symmetric stretching vibrations of coordinated carboxylate groups, respectively, confirming successful metal-ligand complexation. Additionally, the appearance of a peak at 516 cm⁻¹ is attributed to Cu-O stretching vibrations, further validating the formation of the Cu-MOF framework. These observations are consistent with previous studies on Cu-MOFs synthesized from BTC ligands [17].

X-ray photoelectron spectroscopy (XPS), as shown in **Figure 2f**, was employed to analyze the surface composition and chemical states of the synthesized Cu-MOF. The elemental profile revealed Cu, O, and C with atomic percentages of 22.25%, 51.95%, and 25.80%, respectively. The Cu 2p peak, located at 934.6 eV, is indicative of the Cu^{2+} oxidation state, commonly observed in copper-based coordination frameworks. The O Is signal at 532.5 eV arises from oxygen atoms within carboxylate groups and possibly adsorbed water or hydroxyl species. The C Is peak at 284.8 eV corresponds to both aromatic and carboxylic carbon from the BTC ligand. These binding energies and atomic ratios support the successful formation of the Cu-MOF network and align with previously reported results for Cu-BTC structures [18].

As shown in Figure 2g, the zeta potential of the synthesized Cu-MOF exhibits a strong dependence on pH, transitioning from positive values in acidic environments to negative values under alkaline conditions. This variation reflects changes in surface charge due to the gradual loss of protons from functional groups such as carboxylates as the pH increases. The point of zero charge (PZC) was observed at a pH of approximately 4.0, indicating the condition under which the surface of the Cu-MOF becomes electrically neutral. This behavior is typical of metalorganic frameworks containing carboxylic acid-based linkers and plays a key role in modulating interactions with charged species in solution.

The specific surface area of the synthesized Cu–MOF was evaluated using N_2 adsorption–desorption isotherms at 77 K, and the Brunauer–Emmett–Teller (BET) method was applied in the relative pressure range $p/p_0 = 0.05$ –0.3 (Figure 2h). The BET plot shows a well-defined linear region, indicating the validity of the BET model for this MOF. Cu-MOF surface area was found to be 5.10 m²/g with a total pore volume of 6.09×10^{-2} cm³/g, and a mean pore diameter of 47.73 nm. These results indicate that the adsorbent exhibits limited accessible porosity to N_2 , with uptake primarily arising from interparticle holes and macropores [19]. These large pores can still facilitate the diffusion of dye molecules toward the external surface and active adsorption sites, even though the basic microporosity of the framework is not accessible under N_2 adsorption conditions.

3.2. Thermal Stability

The thermal stability of the Cu-MOF was evaluated by TGA analysis under a nitrogen atmosphere (**Figure 2i**). The figure shows a weight loss of about 12.27% below 150°C; this loss can be due to the removal of adsorbed water molecules and residual solvents within the porous framework. The second loss occurs between 200 and 450°C, corresponding to a 12.56% loss. The second loss corresponds to the decomposition of the organic linker and destruction of the MOF structure. There is a minor weight loss observed above 450 °C of 1.12%, which may be associated with further breakdown of carbonaceous residues. Additionally, a high residual mass of approximately 74% remains at 1000°C, indicating the presence of stable copper oxide species as the final decomposition product, which confirms the high thermal stability of the Cu-MOF.

3.3. Optimization of Adsorption Factors

3.3.1. pH of the Solution

Solution pH significantly affects adsorption by altering both the surface charge of the Cu-MOF adsorbent and the ionization state of the dyes, as shown in **Figure 3a**. In this study, maximum removal efficiency (Re%) was observed at pH 3 for the anionic dyes *CR* and *TOO*. Under acidic conditions, the Cu-MOF surface becomes positively charged due to protonation, thereby enhancing electrostatic attraction with negatively charged dyes, such as *CR* and *TOO*. As the pH increases, the surface charge becomes less favorable for anionic dye adsorption due to reduced electrostatic interactions [20].

3.3.2. Contact Time

Figure 3b shows how contact time influences the removal of *TOO* and *CR* dyes. The removal efficiency (Re%) increases with time until it levels off, suggesting that the adsorption sites on the Cu-MOF become fully occupied. This trend reflects the adsorption process's reliance on contact duration. Selecting an optimal contact time is crucial for achieving effective dye removal while maintaining an efficient process [21].

3.3.3. Effect of Mass

Figure 3c illustrates that increasing the amount of Cu-MOF adsorbent enhances the availability of active sites, thereby promoting the removal of *CR* and *TOO* dyes. However, as the adsorbent mass continues to rise, the ratio between dye molecules and available binding sites diminishes, leading to a decline in adsorption capacity (q_e). While a higher dosage typically results in better removal efficiency (%Re) due to more active sites, excessive amounts of adsorbent contribute little additional benefit. This effect may be attributed to site saturation or particle aggregation, which can limit the effective surface area available for adsorption. Thus, determining an optimal adsorbent dosage is crucial for achieving efficient dye removal while minimizing material usage and maintaining high performance [22].

3.3.4. Dye Concentration

The influence of initial dye concentration on the adsorption efficiency of Cu-MOF was examined for the removal of *CR* and *TOO* dyes, as shown in **Figure 3** (d,e). This investigation was conducted by varying the initial dye concentration while maintaining other parameters, such as pH, temperature, contact time, and adsorbent dosage, at constant levels. At lower

concentrations, Cu-MOF demonstrated high removal efficiency for both dyes. However, as the initial concentration increased, a noticeable decrease in removal efficiency was observed. This decline is likely due to the saturation of available active sites on the Cu-MOF surface, which restricts adsorption at higher concentrations. The reduced performance at elevated concentrations can also be attributed to intensified competition among dye molecules for limited binding sites. These findings highlight the importance of regulating initial concentrations to enhance removal effectiveness and ensure the efficient utilization of the adsorbent [23].

3.3.5. Temperature

As illustrated in **Figure 3f**, temperature has an apparent effect on the adsorption efficiency of *CR* and *TOO* dyes using Cu-MOF. Higher temperatures increase the mobility of dye molecules, enhancing their ability to access and bind to active sites within the adsorbent. *CR* achieves its highest removal efficiency at 35°C, while *TOO* exhibits optimal adsorption at 40°C, indicating that moderate increases in temperature can enhance the uptake of dyes. However, beyond these optimal points, adsorption efficiency begins to decline, likely due to weaker interactions between the dye molecules and the adsorbent surface or the onset of desorption. These results highlight the importance of maintaining suitable temperature conditions to achieve optimal adsorption performance [24].

3.3.6. FT-IR analysis of adsorbed dyes onto Cu-MOF

As shown in Figure 4, FTIR spectroscopy was employed to investigate the structural features of Cu-MOF before and after adsorption of CR and TOO dyes. The characteristic bands of the pristine Cu-MOF appeared at 3400 cm⁻¹ (O-H stretching), 1564 cm⁻¹ (asymmetric stretching of carboxylate groups), 1411 cm⁻¹ (symmetric stretching of carboxylates), and 516 cm⁻¹ (Cu-O vibrations), confirming the formation of MOF with coordinated carboxylate ligands. Upon interaction with the CR dye, distinct spectral changes were observed. The O-H stretching shifted from 3400 cm⁻¹ to 3350 cm⁻¹, indicating hydrogen bonding or coordination interactions between dye molecules and the MOF. A new band appeared at 1616 cm⁻¹, attributed to N=N azo stretching from the CR dye. Additional bands at 1083 cm⁻¹ and 628 cm⁻¹ correspond to the presence of sulfonate groups and other functional groups in the dye, confirming successful adsorption. The reduction in intensity of the band at 516 cm⁻¹ suggests a potential alteration in the Cu-O environment due to interaction with dye molecules. Similarly, after adsorption of the TOO dye, the FTIR spectrum exhibited notable shifts. The broad O-H band slightly shifted from 3400 cm⁻¹ to 3340 cm⁻¹. New absorption bands appeared at 1637 cm⁻¹ (N=N stretching), 1377 cm⁻¹ (aromatic C=C bending), and 1089 cm⁻¹, indicating the presence of the dye's functional groups within the MOF structure. A band at 605 cm⁻¹ further confirmed the incorporation of dye molecules. Importantly, the sulfate vibration at 1120 cm⁻¹ observed in the free TOO spectrum disappeared after adsorption, suggesting its involvement in binding to the MOF [25].

Overall, the changes in spectral features before and after adsorption confirm the successful interaction of both CR and TOO dyes with the Cu-MOF framework, involving hydrogen bonding, electrostatic interactions, and possible coordination with metal centers.

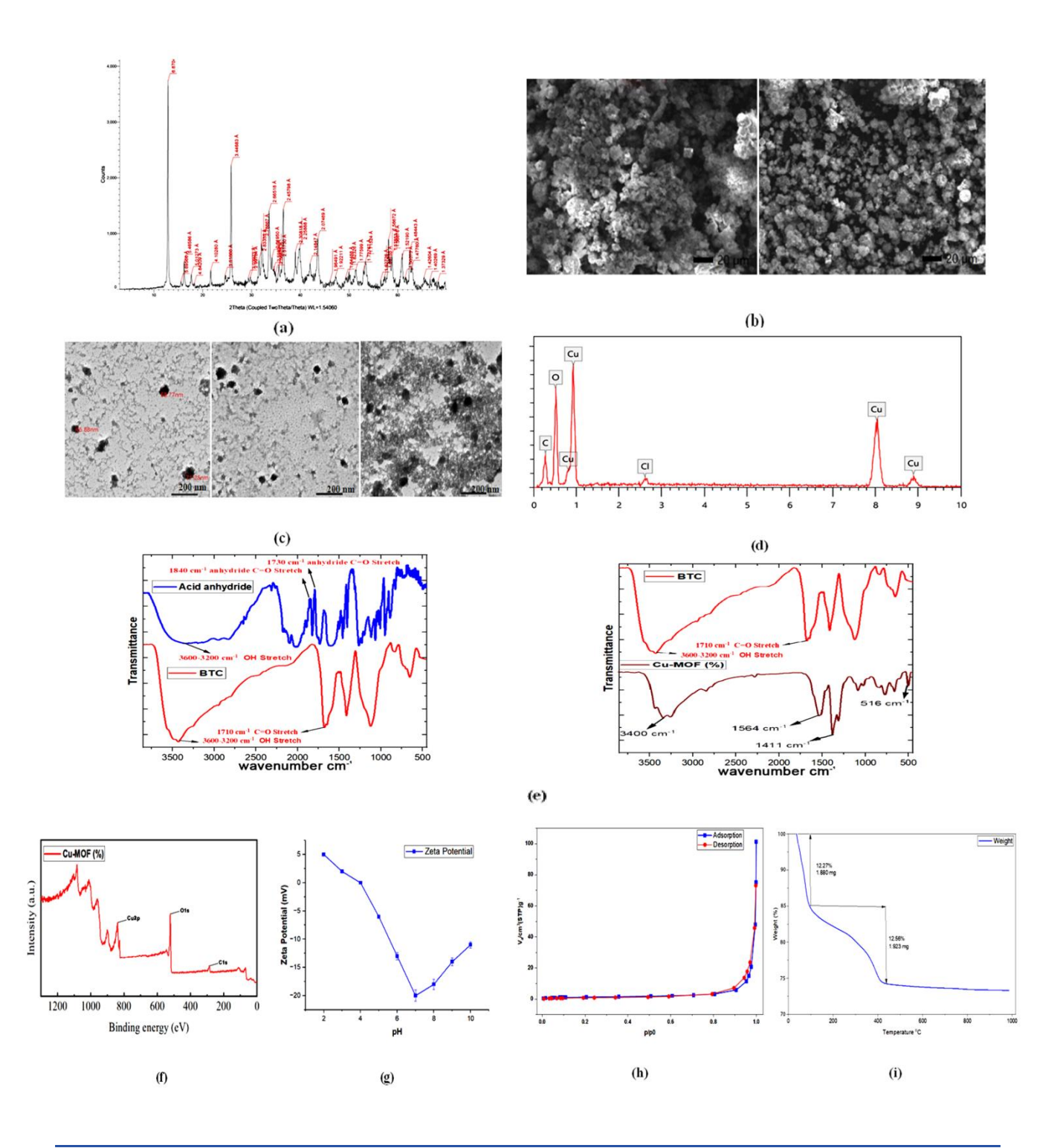


Figure 2. Cu-MOF characterization: (a) XRD pattern, (b) SEM image, (c) TEM image, d) EDX spectrum, (e) XPS spectrum, (f) FT-IR spectrum, (g) Zeta Potential analysis, (h) N2 adsorption-desorption isotherm, and (i) TGA curve.

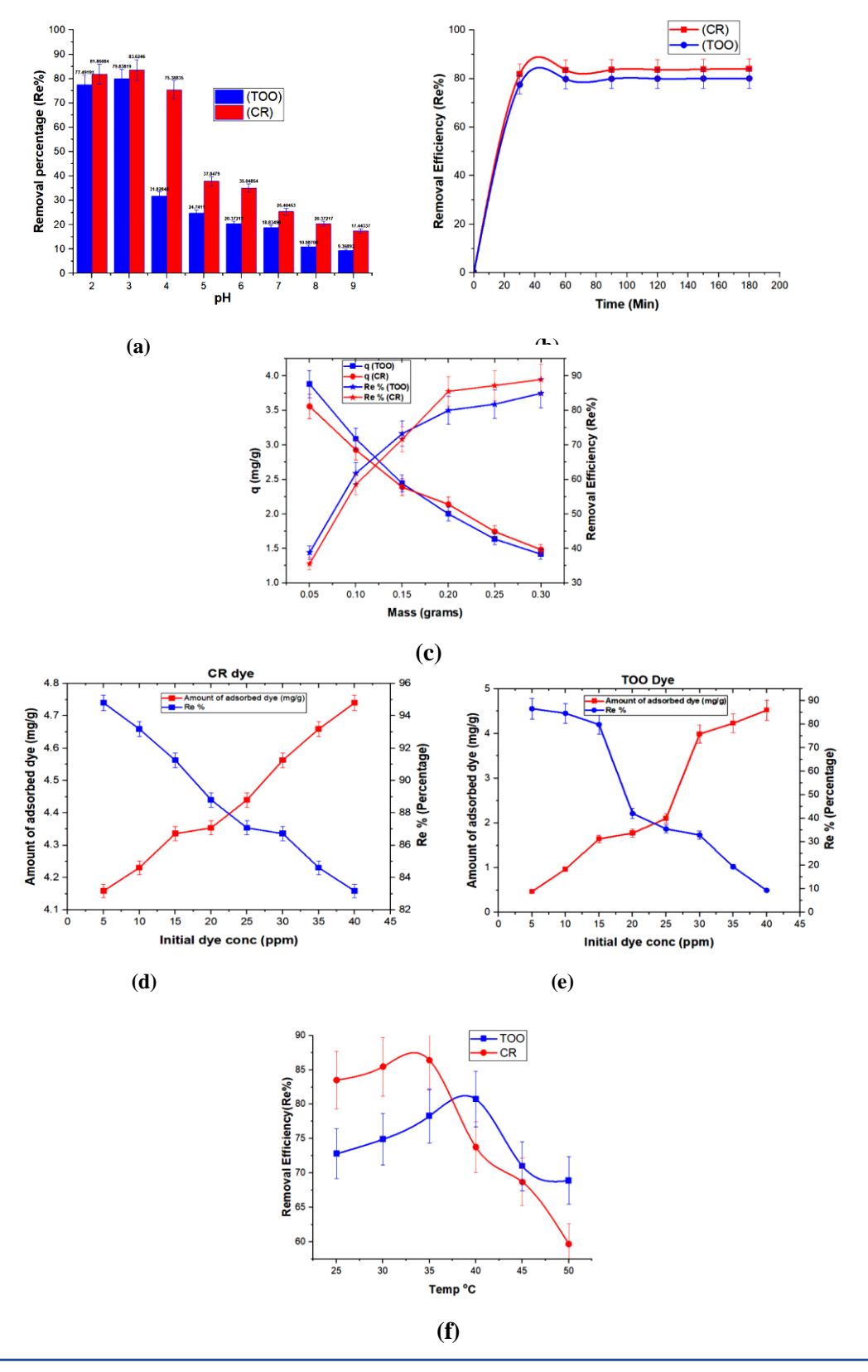


Figure 3. Effect of different operating parameters on dye removal using Cu-MOF: (a) pH, (b) Time, (c) Adsorbent dose, (d&e) Initial dyes concentration, (f) Temperature.

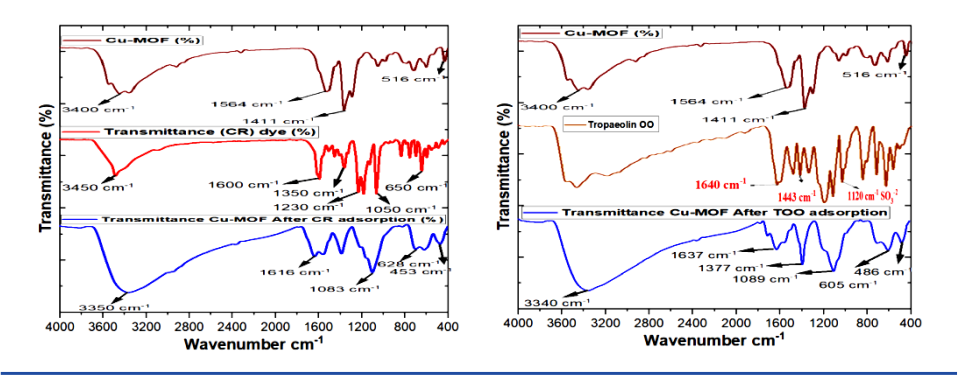


Figure 4. FT-IR spectra before and after dye adsorption of CR and TOO dyes by Cu-MOF.

3.3.7. XPS Analysis of Adsorbed Dyes onto Cu-MOF

X-ray photoelectron spectroscopy (XPS) was used to investigate the surface elemental composition and chemical states of Cu-MOF before and after dye adsorption (Figure 5). The survey spectrum of pristine Cu-MOF reveals prominent peaks corresponding to Cu 2p, O 1s, and C 1s, indicating the presence of copper, oxygen, and carbon as the primary elements in the framework. The Cu 2p signal, centered at 934.6 eV, is characteristic of Cu²⁺ species, confirming the typical oxidation state of copper in MOF. The O 1s peak observed near 532.5 eV is attributed to oxygen in carboxylate groups and potentially surface-bound hydroxyl or water species. The C Is peak at 284.8 eV reflects contributions from both aromatic and carboxylic carbons in the BTC linker. After the adsorption of CR and TOO dyes, noticeable changes are observed in the XPS spectra. New peaks and increased intensities, particularly in the Na 1s and S 2p regions, confirm the successful uptake of the sulfonated dyes, which contain sodium and sulfur groups. These elements are not present in the pristine Cu-MOF, supporting the dye loading. The post-adsorption spectra of CR and TOO also show shifts in the Cu 2p and O 1s binding energies, suggesting interactions between the dye molecules and the active sites on the Cu-MOF surface [26].

3.4. Adsorption kinetics and isotherm studies

Adsorption isotherms and kinetic models are essential tools for elucidating the mechanisms governing the adsorption process. Three adsorption models were used to discuss the removal process, as listed in Table S1, and their linear and non-linear representations are illustrated in Figures S1 & S2. Table 1 shows the results of isotherm studies and the kinetics of the removal process. The Temkin isotherm model best represents the adsorption behavior of both CR and TOO dyes. This suggests a uniform distribution of adsorption energies and potential interactions among adsorbed species on the Cu-MOF surface. The kinetic data (Table 1) for both dyes align closely with the pseudo-second-order model, indicating that chemisorption likely controls the rate of adsorption. The linear and non-linear plots are represented in Figures S3 & S4. The equilibrium adsorption capacities (qe) predicted by the model are consistent with experimental findings, validating the model's suitability. Furthermore, CR exhibited a higher adsorption capacity compared to TOO, reflecting a stronger affinity between CR molecules and the Cu-MOF under the experimental conditions.

These findings underscore the influence of dye structure on adsorption performance and support the effectiveness of Cu-MOF as an adsorbent for azodyes [27].

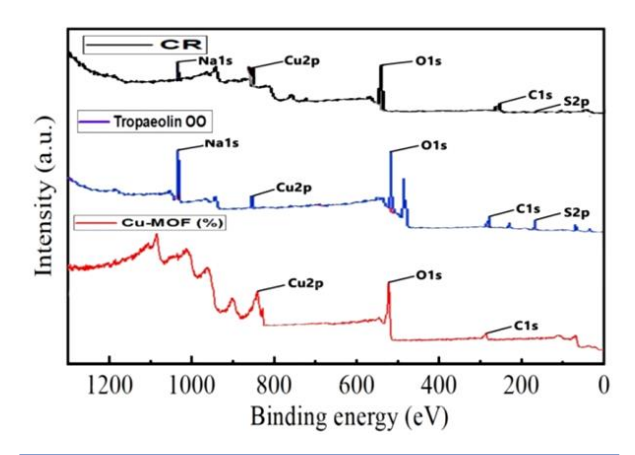


Figure 5. XPS before and after adsorption of *CR* and *TOO* by Cu-MOF.

3.5. Thermodynamic investigations

Thermodynamic analysis reveals variations in adsorption behavior and interaction mechanisms between the dyes and Cu-MOF, reflecting distinct affinities and binding patterns. [28]. The values of Gibbs free energy (ΔG°), enthalpy (ΔH°), and entropy (ΔS°) were derived using established thermodynamic equations described in Table S1, and the Van't Hoff plots were used to derive these parameters for both dyes (Figure S5).

As shown in Table 2, the Gibbs free energy change (ΔG°) for both dyes becomes more negative with increasing temperature, indicating that the adsorption processes are spontaneous and increasingly favorable at elevated temperatures. For both dyes, TOO and CR, the positive values of enthalpy (ΔH°) and entropy (ΔS°) suggest that the adsorption is endothermic and associated with increased randomness at the solid–liquid interface. This may reflect greater molecular mobility or structural reorganization during the binding process. These distinct thermodynamic profiles emphasize the role of dye structure in influencing the adsorption mechanism and the thermal sensitivity of the process.

Table1. Adsorption isotherm and kinetic models for dye adsorption on Cu-MOF

Model	Parameters	CR	TOO					
Adsorption isotherm								
Langmuir	$K_L(L/mg)$	0.0158	0.00138					
	\mathbb{R}^2	0.469	0.884					
	q _{max} (mg g ⁻¹)	2.189563	2.877832					
Freundlich	n	2.030	5.92					
	$K_F*10^{-2}(mg/g) (L/mg)^{1/n}$	1.851	1.416					
	\mathbb{R}^2	0.592	0.784					
	B _T (J mol ⁻¹)	0.248	0.562					
Temkin	$K_T (L mg^{-1})$	0.510	4.49					
	\mathbb{R}^2	0.977	0.959					
Kinetics								
1 st order	q _{exp} (mg/g)	2.282	2.291					
	\mathbf{k}_1	0.020	0.030					
	\mathbb{R}^2	0.515	0.712					
	q_{e}	8.19	7.24					
2 nd order	k_2	1.1	1.8					
	R^2	1	1					
	q_{e}	2.3562	2.3758					

Table2. Thermodynamic parameters for dye removal by Cu-MOF.

Temp. (K)	CR			TOO		
	$\Delta G^{\circ}(\mathrm{kJ.mol}^{-1})$	ΔH°(kJmol ⁻¹)	$\Delta S^{\circ}(\mathrm{J\ mol^{-1}K^{-1}})$	$\Delta G^{\circ}(\mathrm{kJmol^{-1}})$	ΔH°(kJmol ⁻¹)	ΔS°(J mol ⁻¹ K ⁻¹)
298	-0.654	35.20	120.3	-0.667	19.24	68.85
303	-1.205			-1.081		
308	-1.905			-1.782		
313	-2.609			-2.468		
318	-2.954			-1.653		

3.6. Reusability and regeneration of Cu-MOF

The regeneration study demonstrated a gradual decline in the adsorption efficiency of Cu-MOF over repeated use. In the initial cycle, the removal efficiency (%Re) for the dye reached 89%. Following the first, second, third, fourth, and fifth regeneration cycles, the efficiency decreased to approximately 86%, 81%, 76%, 71%, and 66% respectively. The regeneration efficiencies, calculated according to Equation 3, were found to be 96.63%, 94.19%, 93.83%, 93.42%, and 92.96% for the first to fifth cycles, respectively. This decline in performance suggests a partial loss of adsorption capacity over time. The reduction may be attributed to the gradual degradation or

deactivation of active sites on the Cu-MOF surface, as well as potential material loss during the regeneration process. These findings highlight the importance of evaluating adsorbent stability for practical applications and support the potential of Cu-MOF as a recyclable, though not indefinitely reusable, material for dye removal [29].

 $Regeneration \ Efficiency =$

$$\left[\frac{\textit{Removal Efficiency of current cycle}}{\textit{Removal Efficiency of previous cycle}} \times 100\right] \tag{3}$$

3.6.1. EDX analysis of regenerated Cu-MOF

Figure 6 shows the EDX of the regenerated Cu-MOF. The post-

regeneration elemental analysis reveals a composition closely resembling that of the initially synthesized Cu-MOF, indicating that the core elements remained largely preserved after adsorption and regeneration. This consistency suggests that the Cu-MOF framework maintains its chemical integrity through repeated use. Minor deviations in elemental percentages may result from slight material loss or surface alterations during the regeneration process. Overall, the stable elemental profile underscores the structural robustness of Cu-MOF and its potential for reuse in multiple adsorption cycles.

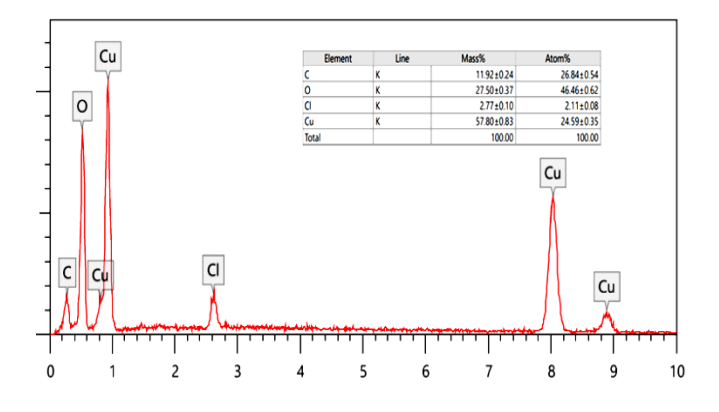


Figure 6. EDX of regenerated Cu-MOF.

3.6.2. FTIR analysis of regenerated Cu-MOF

The FTIR spectra of the Cu–MOF before and after regeneration exhibit the characteristic vibrational bands associated with the framework. Before regeneration, As shown in **Figure 7**, the spectrum shows a broad band at 3400 cm⁻¹, attributed to O–H stretching vibrations from coordinated water and/or adsorbed moisture. Strong absorptions at 1564 cm⁻¹ and 1411 cm⁻¹ correspond to the asymmetric and symmetric stretching modes of the coordinated carboxylate groups, respectively, confirming successful coordination of the 1,2,4-benzene-tricarboxylate linker to the Cu(II) centers. A distinct band at 516 cm⁻¹ can be assigned to Cu–O stretching vibrations of the metal–ligand cluster.

After regeneration, the FTIR spectrum retains all major characteristic peaks with only slight shifts. The O–H band appears at 3418 cm⁻¹, while the carboxylate stretches are observed at 1589 cm⁻¹ and 1423 cm⁻¹, and the Cu–O vibration is at 523 cm⁻¹. These minor shifts suggest that the framework structure is preserved mainly during the regeneration process, with only subtle changes in local bonding environments, possibly due to the removal of guest molecules and the rearrangement of hydrogen-bonding interactions. The close agreement between the spectra before and after regeneration demonstrates the structural stability and reusability of the Cu–MOF, a key requirement for adsorption and catalytic applications.

3.7. Comparative Adsorption Studies on Dves Using MOFs

It is essential to highlight that the adsorption capacity (q_e) values are strongly influenced by the experimental conditions, particularly the initial dye concentration. In our study, we deliberately employed relatively low starting concentrations (5–50 mg L^{-1}) to mimic realistic wastewater scenarios. Under such

conditions, the number of dye molecules available per unit mass of adsorbent is inherently lower, resulting in smaller q_e values compared to reports that use much higher initial concentrations (often 200–500 mg L⁻¹ or more). It should be noted, however, that while the calculated adsorption capacity is lower, the removal efficiency (%R_e) remains very high, demonstrating the excellent affinity of Cu-MOF for both CR and TOO dyes. Thus, the smaller qe in our system does not reflect weaker performance but rather highlights the more stringent and practical conditions under which the experiments were conducted. Moreover, these findings provide a more realistic assessment of the applicability of Cu-MOF in treating real effluents, where dve concentrations are generally closer to the levels tested in our work. A comparison of the obtained adsorption capacities with previously reported values is summarized in Table 3, further confirming the competitive performance of Cu-MOF under realistic operational conditions.

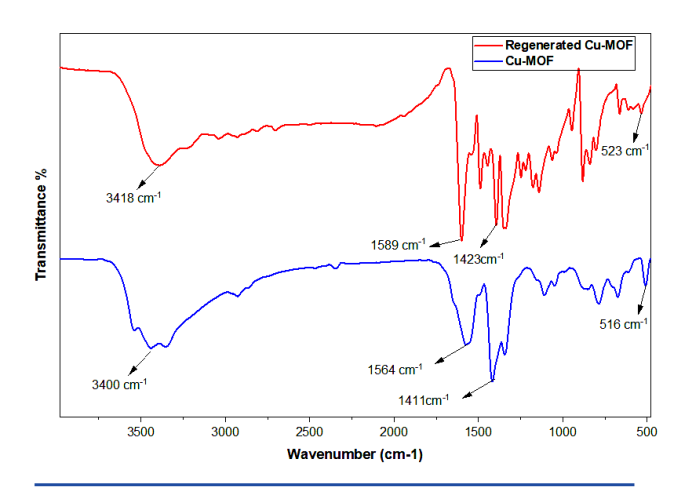


Figure 7. FTIR of regenerated Cu-MOF.

Table 3. Comparison of the adsorptive capacities of Cu-MOF with other studies

Type of MOF	Dye(s)	Initial Concentration (mg/L)	Adsorption Capacity q _e (mg/g)	Reference
(Cu-BTC MOF with Ni/Co decoration)	Congo Red (CR)	25–200	200–250	[19]
This work (Cu-MOF)	Congo Red (CR), Tropaeolin OO (TOO)	5-50	2.3562 (CR) 2.3758 (TOO)	This study
(CuCl ₂ - MOF-5)	Congo Red (CR)	50-300	up to ~400	[21]
(UiO-66, mesoporous analogue)	Anionic & Cationic dyes	20–200	120–180	[28]
(Fe-MIL- 88NH ₂ MOF)	Congo Red (CR)	25–250	180–220	[30]

4. Conclusion

In this work, Cu-MOF was synthesized using Cu(NO₃)₂·3H₂O and 1,2,4-benzenetricarboxylic acid as a new organic linker, resulting in a multifunctional material effective for water purification. The Cu-MOFs showed high adsorption efficiency for textile dyes such as Congo Red and TOO, with removal efficiencies up to 89% and 85% for *CR* and *TOO*, respectively, under optimum conditions. Structural characterizations showed the materials' high crystallinity, porosity, and electrostatic affinity towards anionic dyes. The adsorption process was governed by pseudo-second-order kinetics. It fitted the Temkin isotherm model, indicating a heterogeneous adsorption process involving adsorbate-adsorbent interactions, as supported by both the kinetics and isotherm studies. These findings demonstrate the potential of Cu-MOF as a sustainable adsorbent capable of targeting organic pollutants in wastewater.

Conflict of Interest

The authors declare that the research was conducted in the absence of any commercial or financial relationships that could be construed as a potential conflict of interest.

Availability of data and materials

All data generated or analyzed during this study are included in this manuscript.

Acknowledgement

The authors would like to extend their sincere appreciation to the Science, Technology, and Innovation Funding Authority (STDF) (ID: 46267).

Competing Interests

The authors declare no relevant financial or non-financial interests.

Author Contributions

Mohamed Hagar: Conceptualization, Methodology, Formal analysis, and Supervision. Amira Hossam Eldin: Writing — Original Draft, Review & Editing, and Supervision. Azza Shaker: Visualization, Validation, Investigation, Data Curation, and Supervision. Hanaa Rasheed and Ahmed R. Rabee: Investigation, organic Data Analysis, Writing. Marawan M. Ramadan: Validation, Methodology, Investigation, Data Curation, Writing - Review & Editing.

References

- [1] Bhatnagar, A., &Sillanpää, M. (2010). Utilization of agro-industrial and municipal waste materials as potential adsorbents for water treatment—A review. Chemical Engineering Journal, 157(2–3), 277–296. https://doi.org/10.1016/j.cej.2010.01.007.
- [2] Zhao, S.; Zhu, L.; Chen, Y.; Xu, Y.; Li, H.; Luo, J.; Li, B. Microwave-assisted hydrothermal assembly of 2D copper-porphyrin metal-organic frameworks for the removal of dyes and antibiotics from water. *Environ. Sci. Pollut. Res.* 2020, 27, 39186–39197. https://doi.org/10.1007/s11356-020-08947-9.
- [3] Gosavi, V. D.; Sharma, S. A general review on various treatment methods for textile wastewater. *J. Environ.*

- *Sci. Comput. Sci. Eng. Technol.* **2014**, *3*, 29–39. https://doi.org/10.1080/09714818.2014.11722269.
- [4] Ghaedi, M.; Nasab, A. G.; Khodadoust, S.; Sahraei, R.; Daneshfar, A. Modeling of competitive ultrasonic-assisted removal of the dyes Methylene Blue and Safranin-O using Fe₃O₄ nanoparticles. *Chem. Eng. J.* **2015**, *268*, 28–37.
 - https://doi.org/10.1016/j.cej.2015.01.062
- [5] Yu, S.; Li, X.; Liu, J.; Zhang, L.; Xu, Y.; Ma, J. Recent advances in metal-organic framework membranes for water treatment: A review. Sci. Total Environ. 2021, 800, 149662.
 - https://doi.org/10.1016/j.scitotenv.2021.149662
- [6] Khan, M. S.; Khalid, M.; Shahid, M. What triggers dye adsorption by metal-organic frameworks? The current perspectives. *Mater. Adv.* **2020**, *1*, 1575–1601. https://doi.org/10.1039/D0MA00252C.
- [7] Du, C.; Wang, Q.; Li, Z.; Guo, X.; Wang, P.; Zhang, H. Fe-based metal-organic frameworks (Fe-MOFs) for organic pollutants removal via photo-Fenton: A review. *Chem. Eng. J.* **2022**, *431*, 133932. https://doi.org/10.1016/j.cej.2022.133932.
- [8] Wang, Q.; Wu, Y.; Zhou, Y.; Huang, Y.; Xie, R.; Li, H. Magnetic amino-functionalized-MOF (M = Fe, Ti, Zr)@COFs with superior biocompatibility: Performance and mechanism on adsorption of azo dyes in soft drinks. *Chem. Eng. J.* 2021, 420, 129955. https://doi.org/10.1016/j.cej.2021.129955.
- [9] Soni, S.; Singh, M.; Kumar, R.; Kumar, S.; Singh, R. Removal of crystal violet from aqueous solution using iron-based metal-organic framework. *Desalin. Water Treat.* 2020, 205, 386–399.
 - https://doi.org/10.5004/dwt.2020.25543.
- [10] Li, R.; Guo, L.; Li, S.; Yu, J.; Xu, Y.; Zhang, Q.; Wang, J. Metal–organic–framework–based materials for antimicrobial applications. *ACS Nano* **2021**, *15*, 3808–3848. https://doi.org/10.1021/acsnano.0c09465
- [11] Aluvala, V.; Matkala, B.; Chilkamarri, S.; Burri, V.; Boggala, S.; Chatla, A.; Inkollu, S.; Aytam, H. P. Synthesis, characterization, and activity evaluation of sulphate-modified Cu-MOF catalyst for the valorization of glycerol to solketal. *Orient. J. Chem.* **2025**, *41*, 506–517.
 - https://doi.org/10.13005/ojc/410220.
- [12] Pach, A.; Podborska, A.; Csapó, E.; Luty-Błocho, M. Tropaeolin OO as a chemical sensor for a trace amount of Pd(II) ions determination. *Molecules* **2022**, 27, 4511. https://doi.org/10.3390/molecules27144511
- [13] Zelenka, T.; Baláž, M.; Férová, M.; Diko, P.; Bednarčík, J.; Királyová, A.; Zauška, E.; Bureš, R.; Sharda, P.; Király, N.; Badač, A.; Vyhlídalová, J.; Želinská, M.; Almáši, M. The influence of HKUST-1 and MOF-76 hand grinding/mechanical activation on stability, particle size, textural properties, and carbon dioxide sorption. *Sci. Rep.* **2024**, *14*, 15386. https://doi.org/10.1038/s41598-024-66432-z.

- [14] Vazirinezhad, K.; Shariatmadar Tehrani, F.; Zeinali, S. Porosity and morphology control of mesoporous Cu-BTC metal-organic framework microparticles. *Prog. Phys. Appl. Mater.* 2024, 4, 47–58. https://doi.org/10.22075/PPAM.2024.33337.1090
- [15] Li, W.; Zhang, J.; Hu, Y.; Chen, X.; Liu, P. Synthesis and characterization of Cu-BTC metal-organic frameworks for adsorption applications. *J. Solid State Chem.* **2021**, 299, 122164. https://doi.org/10.1016/j.jssc.2021.122164.
- [16] Gao, X.; Zhou, H.; Liu, Y.; Fang, S.; Wang, L. Synthesis and characterization of Cu-BTC MOFs for environmental applications. *J. Mol. Struct.* 2020, 1218, 128524. https://doi.org/10.1016/j.molstruc.2020.128524.
- [17] Chen, L.; Sun, Y.; Zhao, W.; Liu, J. XPS study of Cu-BTC MOFs and their interaction with organic molecules. *Surf. Interface Anal.* **2021**, *53*, 744–751. https://doi.org/10.1002/sia.690.3
- [18] Jaksani, B.; Abburi, J.; Islam, H.; Gonuguntla, S.; Baidya, T.; Pal, U. In situ decorated Ni and Co in a CuBTC MOF for synergistic photocatalytic hydrogen generation. *Mater. Adv.* **2025**, *6*, 4211–4219. https://doi.org/10.1039/D4MA01243G
- [19] Echenique-Errandonea, E.; Rojas, S.; Abdelkader-Fernández, V. K.; Pérez-Mendoza, M.; Mendes, R. F.; Barbosa, P.; Seco, J. M. Adsorptive Capacity, Inhibitory Activity and Processing Techniques for a Copper-MOF Based on the 3,4-Dihydroxybenzoate Ligand. *Molecules* 2022, 27(22), 8073. https://doi.org/10.3390/molecules27228073.
- [20] Wang, J.; Guo, X. Adsorption kinetics and isotherm models of heavy metals by various adsorbents: An overview. *Crit. Rev. Environ. Sci. Technol.* **2023**, *53*, 1837–1865. https://doi.org/10.1080/10643389.2023.2221157
- [21] Mosavi, S. H.; Zare-Dorabei, R.; Bereyhi, M. R. Rapid and effective ultrasonic-assisted adsorptive removal of Congo Red onto MOF-5 modified by CuCl₂ in ambient conditions: Adsorption isotherms and kinetics studies. *ChemistrySelect* **2021**, *6*, 4432–4439. https://doi.org/10.1002/slct.202100540.
- [22] Alsaiari, R. A.; Alam, M. M.; Alzahrani, F. M.; Aldalbahi, A.; Alotaibi, B. S.; Alshehri, A. Camel bone-derived hydroxyapatite as a green adsorbent for Methylene Blue removal: Effect of dosage and mechanistic insights. *Pol. J. Environ. Stud.* **2025**, *34*, 1–12. https://doi.org/10.15244/pjoes/207656.
- [23] Dahlan, I.; Kurniawan, A.; Jamil, N.; Huda, N.; Wahid, H. Modelling of batch organic dye adsorption using modified metal—organic framework 5 (MOF-5): Investigating effects of initial dye concentration. *AIP Conf. Proc.* 2023, 2650, 040009. https://doi.org/10.1063/5.0147966.
- [24] Liang, J.; Liu, Y.; Chen, W.; Li, Y.; Wang, Z. Thermodynamic and kinetic insight into Congo Red

- adsorption onto activated carbon derived from water hyacinth: Effect of temperature. *J. Environ. Chem. Eng.* **2021**, *9*, 104333.
- https://doi.org/10.1016/j.jece.2020.104333
- [25] Ahmad, M.; Yasin, T.; Rehman, S.; Iqbal, M. FTIR and XRD analysis of Cu-based metal—organic frameworks before and after adsorption of azo dyes: Insights into interaction mechanisms. *J. Mol. Struct.* **2020**, *1215*, 128220.
 - https://doi.org/10.1016/j.molstruc.2020.128220
- [26] Patil, Y. A.; Shankarling, G. S. Deep eutectic solvent—mediated, energy-efficient synthesis of copper terephthalate metal-organic framework and its application in degradation of an azo dye. *Chem. Eng. J. Adv.* **2020**, *3*, 100032.
 - https://doi.org/10.1016/j.ceja.2020.100032
- [27] Chen, B.; Xiao, S.; Zhao, H.; Li, X.; Xie, Y.; Wang, J. High-efficient removal of anionic dye from aqueous solution using MOF-525@CS aerogel. *Int. J. Biol. Macromol.* **2024**, 256, 128433.
 - https://doi.org/10.1016/j.ijbiomac.2023.128433.
- [28] Hidayat, A. R. P.; Zulfa, L. L.; Widyanto, A. R.; Abdullah, R.; Kusumawati, Y.; Ediati, R. Selective adsorption of anionic and cationic dyes on mesoporous UiO-66 synthesized using a template-free sonochemistry method: Kinetic, isotherm and thermodynamic studies. *RSC Adv.* 2023, *13*, 12320–12343. https://doi.org/10.1039/D2RA06947D.
- [29] Al-Omari, M. H.; Abu-Rayyan, A.; Ragab, A. H.; Taher, M. A.; El-Sayed, E. M.; Elfiky, A.; Taha, A.; Mahmoud, F. Optimized Congo Red dye adsorption using ZnCuCr-based MOF for sustainable wastewater treatment. *Langmuir* 2025, 41, 5947–5961. https://doi.org/10.1021/acs.langmuir.4c04661.
- [30] Fu, Q.; Lou, J.; Zhang, R.; Peng, L.; Zhou, S.; Yan, W.; Mo, C.; Luo, J. Highly effective and fast removal of Congo Red from wastewater with metal-organic framework Fe-MIL-88NH₂. *J. Solid State Chem.* **2021**, 294, 121836.
 - https://doi.org/10.1016/j.jssc.2020.121836.